Dysfunction of calcium-regulated exocytosis at a single-cell level causes catecholamine hypersecretion in patients with pheochromocytoma

Sébastien Houy, Laura Streit, Inès Drissa, Marion Rame, Charles Decraene, Sophie Moog, Laurent Brunaud, Joël Lanoix, Rabie Chelbi, Florence Bihain, et al.

Dysfunction of calcium-regulated exocytosis at a single-cell level causes catecholamine hypersecretion in patients with pheochromocytoma.

Sébastien Houy[1*], Laura Streit[1*], Inès Drissa[2], Marion Rame[1], Charles Decraene[1,10], Sophie Moog[1], Laurent Brunaud[3], Joël Lanoix[4], Rabie Chelbi[1,7], Florence Bihain[3], Stéphanie Lacomme[5], Sandra Lomazzi[5], Philippe Campoli[6], Michel Vix[8], Didier Mutter[8], Eustache Paramithiotis[9], Christophe Dubessy[2,11], Nicolas Vitale[1], Stéphane Ory[1#] and Stéphane Gasman[1#§]

[1]*Centre National de la Recherche Scientifique, Université de Strasbourg, Institut des Neurosciences Cellulaires et Intégratives, F-67000 Strasbourg, FRANCE.*
[2] *Univ. Rouen, INSERM, Normandie Univ., Différenciation et Communication Neuroendocrine, Endocrine et Germinale, F-76000 Rouen, FRANCE.*
[3]*Département de Chirurgie Viscérale, Métabolique et Cancérologique (CVMC), INSERM NGERE-U1256, Université de Lorraine, CHRU NANCY, Hôpital Brabois adultes, F-54511 Vandœuvre-lès-Nancy, FRANCE.*
[4]*Institut de Recherche en Immunologie et en Cancérologie (IRIC), Université de Montréal, Montréal, QC H3C 3J7, Canada, Département de Médecine, Université de Montréal, Montréal, QC H3C 3J7, CANADA.*
[5]*Centre de Ressources Biologiques Lorrain, CHRU Nancy, Hôpitaux de Brabois, F-54511 Vandœuvre-lès-Nancy, FRANCE.*
[6]*Department of Biopathology, CHRU-ICL, CHRU Nancy, F-54511 Vandoeuvre-lès-Nancy, FRANCE and Faculty of Medicine, Université de Lorraine, F-54511 Vandoeuvre-lès-Nancy, FRANCE.*
[7]*Inovarion, F-75005 Paris, FRANCE.*
[8]*NHC Strasbourg, Service de Chirurgie Digestive et Endocrinienne des Hôpitaux Universitaires de Strasbourg, Hôpital Civil, F-67000 Strasbourg, FRANCE.*
[9]*CellCarta Biosciences, Inc., Montréal, Québec, CANADA H2X 3Y7.*
[10]*Centre National de la Recherche Scientifique, Université de Strasbourg, Laboratoire de Neurosciences Cognitives et Adaptatives, F-67000 Strasbourg, FRANCE.*
[11] *Univ. Rouen, INSERM, CNRS, HERACLES, PRIMACEN, F-76000 Rouen, FRANCE.*

* S. Houy and L. Streit contributed equally to this paper
\# S. Ory and S. Gasman contributed equally to this paper
§ Corresponding author: Stéphane Gasman, address as above
e-mail: gasman@inci-cnrs.unistra.fr

Running title: Secretory activity of human pheochromocytoma cells

Key words: calcium-regulated exocytosis, neuroendocrine secretion, pheochromocytoma, carbon fiber amperometry, mass spectrometry

Abstract

Neuroendocrine tumors constitute a heterogeneous group of tumors arising from hormone-secreting cells and are generally associated with a dysfunction of secretion. Pheochromocytoma (Pheo) is a neuroendocrine tumor that develops from chromaffin cells of the adrenal medulla, and is responsible for an excess of catecholamine secretion leading to severe clinical symptoms such as hypertension, elevated stroke risk and various cardiovascular complications. Surprisingly, while the hypersecretory activity of Pheo is well known to pathologists and clinicians, it has never been carefully explored at the cellular and molecular levels. In the present study, we have combined catecholamine secretion measurement by carbon fiber amperometry on human tumor cells directly cultured from freshly resected Pheos, with the analysis by mass spectrometry of the exocytotic proteins differentially expressed between the tumor and the matched adjacent non-tumor tissue. In most patients, catecholamine secretion recordings from single Pheo cells revealed a higher number of exocytic events per cell associated with faster kinetic parameters. Accordingly, we unravel significant tumor-associated modifications in the expression of key proteins involved in different steps of the calcium-regulated exocytic pathway. Altogether, our findings indicate that dysfunction of the calcium-regulated exocytosis at the level of individual Pheo cell is a cause of the tumor-associated hypersecretion of catecholamines.

1. Introduction

Through the secretion of hormones and neuropeptides, the neuroendocrine system controls many vital functions such as metabolism, blood pressure, reproduction, growth and development, stress and eating behaviors, to only cite a few. Neoplasms can derive from all kinds of hormone secreting cells giving rise to a neuroendocrine tumor (NET). Thus, the NETs constitute a highly heterogeneous group of neoplasms, but share a common feature in that they are often associated with a deregulation of hormone secretion, mainly hypersecretion, which can induce symptoms and major clinical complications [1]. Therefore, the secretory pathways and their dysfunctions appear as an important issue to be considered in NETs. However, the cellular and molecular mechanisms underlying hypersecretory activity of NETs remain poorly known.

In neuroendocrine cells, hormones and neuropeptides are stored in large dense core vesicles (secretory granules) and are secreted through calcium-regulated exocytosis, a process that has been intensively studied for decades [2]. It involves several tightly regulated trafficking steps including the recruitment of the secretory granules to the cell periphery, their docking to exocytic sites of the plasma membrane, their priming and finally the fusion between the secretory granule membrane and the plasma membrane leading to the release of the intra-granular content [3, 4]. Chromaffin cells of the adrenal medulla, which store and then secrete catecholamines into the blood stream, have been widely used by us and others as an experimental model to uncover the molecular mechanisms controlling calcium-regulated exocytosis [5-7].

The NETs deriving from chromaffin cells of the adrenal medulla are called pheochromocytomas (Pheos) [8]. Most of the Pheos are responsible for catecholamine hypersecretion leading to clinical symptoms such as permanent or paroxysmal hypertension or to cardiovascular complications including myocarditis, Takotsubo syndrome and various forms of cardiomyopathies [8-11]. The reason for this excess of secretion is currently not known. Among the likely possibilities are an anarchic proliferation of secretory cells and/or an intensification of the secretory capacity at the single cell level. We therefore attempted to investigate the cellular mechanisms responsible for a possible specific secretory dysfunction in Pheos by performing carbon fiber amperometry on primary culture of human Pheo cells. This technique allows the precise measurement, in single cell, of individual exocytotic event dynamics in real time [12, 13]. Combined with the detection, by mass spectrometry, of the expression change of exocytotic proteins in human Pheo tissues, it allowed us to reveal upregulated exocytosis at the single cell level and to identify specific steps of the exocytotic process that are dysregulated in the tumors, as well as potential actors of the molecular machinery triggering hypersecretion in Pheos.

2. Material and methods

2.1. Subjects and samples

The medical files of patients with Pheo admitted in 2 French centers (CHRU, Nancy and NHC, Strasbourg) between 2004 and 2019 were retrospectively reviewed. We collected initial diagnosis, including a clinical examination looking for hormonal-related symptoms, and biological analysis. As recommended by the Endocrine Society clinical practice guideline published in 2014 [14], genetic testing for Pheo was proposed to patients to identify germline mutations in the major susceptibility genes (SDHB, SDHC, SDHD, VHL, NF1, RET, TMEM127, MAX) using Sanger sequencing and multiplex ligation-dependent probe amplification (MLPA). Then, as recommended in the consensus statement published in 2017 [15], next-generation-sequencing (NGS)-based diagnostic was carried out for the more recent patients. Biological analysis comprised the measurement of metanephrine (MN) and normetanephrine (NMN) levels, in urine and/or plasma. When available, chromogranin A (CGA) measurements were also registered. Levels of free MN, NMN and CGA in plasma, as well as urinary levels of MN and NMN are presented as ratios normalized by the upper limit of normal range (ULN). Plasma and urinary MN or NMN levels reaching two-fold the upper limit of the normal range and/or CGA exceeding the upper limit of the normal range was defined as the threshold of abnormal hormonal secretion [8]. The ULN of free MN and NMN were 0.40 and 0.98 nmol/L in plasma and 1625 and 2620 nmol/24 h in urine, respectively. The upper reference limit for CGA was 100 mg/L. Catecholamine-producing phenotypes of Pheos were categorized as previously described [16]: adrenergic (AD) phenotype, when MN content exceeded 10% of the combined MN and NMN contents, or noradrenergic (NAD) phenotype when MN content remained below 10% of the combined MN and NMN contents. Pathological evaluation was reviewed, including tumor size, Ki-67 index and the PASS (Pheochromocytoma of the Adrenal Gland Scaled Score) as previously described [17]. Biological and clinical characteristics are summarized in Tables 1 and 2 whereas details per patient are described in Supplementary Table 1.

2.2. Primary culture of human pheochromocytoma and non-tumor cells

Human cells were cultured from freshly resected Pheos and non-tumor tissues. This culture was performed according to Moog and collaborators [18] with slight modifications. In the operating room and immediately after the resection, the adrenal gland was cut longitudinally in two parts (see Figure 1) and Pheo and non-tumor parts were identified before sampling. Roughly a 1 cm^3 piece of tumor tissue was dissected and the non-tumor tissue was carefully dissected outside the tumor zone. Pieces were immediately plunged into ice cold transport medium (Ca^{2+}- and Mg^{2+}-free Hank's Balanced Salt Solution (CMF HBSS, Sigma) supplemented with 0.2% Fetal Bovine Serum (FBS, Gibco) and 1% penicillin/streptomycin (Sigma) or MACS Medium Tissue Storage solution (Miltenyi Biotec). Up to 3 hours after resection, the tumor sample was minced into 1 mm^3 pieces in a dish containing CMF HBSS. The non-tumor sample was carefully dissected under a binocular magnifier to isolate the medullary part of the gland. Tumor chunks were collected, centrifuged at 250 g for 5 min at

room temperature and the pellet resuspended in 15 mL of complete medium (RPMI 1640 GlutaMAX^{TM} (Gibco), 15% FBS, 1% penicillin/streptomycin). Red blood cells, debris and fat were separated from minced tissue by sedimentation for 15 min at room temperature. The supernatant was removed and 15 mL of complete medium was added to the pellet before centrifugation at 250 g for 5 min. Tissue pieces were resuspended in HBSS (in 10 times the tissue volume), containing 1.5 mg/mL of collagenase B (Roche) and 1 mg/mL of the protease dispase II (Gibco) and tumor or non-tumor samples gently rocked for 45 min or 20 min at 37°C respectively. Non-tumor samples were gently triturated and incubated with enzymes for an additional 10 min. For tumor samples, 5 min before the end of protease digestion, 0.1 mg/mL DNase I (Roche) was added to remove potential DNA clumps. Tumor and non-tumor samples were left for a few minutes to sediment at room temperature then the supernatant was recovered (first fraction). The pellets were resuspended in 5 mL or 1 mL of CMF HBSS for tumor and non-tumor samples respectively, and triturated for a couple of minutes to dislodge cells from chunks. The remaining pieces were left for a few minutes to sediment and the supernatant was recovered (second fraction). All fractions were centrifuged at 800 g for 5 min at room temperature. Tumor pellets were resuspended in 2 mL of CMF HBSS and 4 mL of Red Blood Cell Lysis Buffer (Roche) was added before being gently rocked for 10 min at room temperature. They were then centrifuged at 500 g for 5 min. Finally the tumor and non-tumor pellets were resuspended into complete medium. Cell viability and density were estimated under a microscope and 300 µL of cell suspension was seeded into type I collagen (Corning)-coated 35 mm dishes (MatTek). Cells were left to adhere overnight at 37°C in an incubator with water-saturated and 5% CO_2 atmosphere. 2 mL of complete RPMI was added the following day and cells were used within two days.

2.3. Carbon fiber amperometry

Human tumor cells from freshly resected Pheo or non-tumor cells were washed with Locke's solution (140 mM NaCl, 4.7 mM KCl, 2.5 mM $CaCl_2$, 1.2 mM KH_2PO_4, 1.2 mM $MgSO_4$, 11 mM glucose, 0.01 mM EDTA and 15 mM HEPES, pH 7.5) and processed for catecholamine release measurements by amperometry as previously described [19, 20]. A carbon fiber electrode of 5 µm diameter (ALA Scientific Instruments) was held at a potential of +650 mV compared with the reference electrode (Ag/AgCl) and approached close to one cell. Secretion of catecholamines was induced by a 10 s pressure ejection of a 100 µM nicotine (Sigma) solution from a micropipette (Femtotips®, Eppendorf) positioned approximately 10 µm from the cell and recorded over 60 s. The amperometric recordings were performed with an AMU130 amplifier (Radiometer Analytical), calibrated at 5 kHz, and digitally low-pass filtered at 1 kHz. Analysis of the amperometric recordings was performed as previously described with a macro (laboratory of Dr. R. Borges; http://webpages.ull.es/users/rborges/) written for Igor software (WaveMetrics), allowing automatic spike detection and extraction of spike parameters [21]. Only cells containing at least 5 spikes are included in the analysis. The spike parameters analysis was restricted to spikes with amplitudes higher than 5 pA, which were considered as exocytic events [13, 22]. All spikes identified by the program were visually inspected. Overlapping spikes and spikes with aberrant shapes were counted in the total number of spikes and then discarded for parameters analysis. Quantal size (spike charge,

Q) of each individual spike was measured by calculating the spike area above the baseline, the spike area being defined as the time integral of each transient current. Imax was defined as the height of each spike, half-width as the width of each spike at half its height ($T_{1/2}$) and T_{peak} as the spike rise time (Figure 1A).

2.4. Tissue fractionation

Frozen tumor and matched non-tumor adjacent tissues were cut into small pieces (~10 mm^3), and 3 mL of homogenization buffer (0.25 M sucrose, 10 mM Tris pH 7.4, 100 units/mL of DNase I, 5 mM $MgCl_2$, complete protease inhibitor EDTA-free cocktail) was added per tissue sample, homogenized twice for 10 s then once for 20 s using a polytron set at speed 4.0. Homogenates were filtered through a 180 µm nylon and brought to 3 mL with the homogenization buffer, if necessary. For each sample, light membranes were obtained by isopycnic centrifugation using discontinuous sucrose gradients in which samples brought to 1.4 M sucrose were layered by 1.2 M and 0.8 M sucrose. After centrifugation at 155,000 g for 2 hours at 4°C, the light membrane fraction located at the 0.8 M to 1.2 M sucrose interface was collected, snap-frozen in liquid nitrogen and stored at -80°C. The light membrane fraction was enriched with plasma membrane, Golgi, endosomes and secretory pathway associated membranes. The cytosol fractions were obtained by centrifuging 200 µL of crude homogenates at 150,000 g for 1 hour at 4°C. The supernatants were collected, snap-frozen and stored at -80°C.
The amount of proteins were determined using the bicinchoninic acid (BCA) assay according to the manufacturer's instructions (Pierce).

2.5. Mass spectrometry analysis

30 µg of samples (homogenates, cytosol or light membranes) was incubated in a denaturing buffer at final concentration of 7 M urea, 175 mM NH_4HCO_3, 8.75% v/v acetonitrile and incubated for 30 min at room temperature. Samples were then diluted to 1 M urea with water and digested with trypsin (Promega) overnight at 37°C at a ratio of 1 µg of trypsin per 10 µg of protein for homogenate and cytosol samples while for light membranes, the ratio was set at 1 µg of trypsin per 25 µg of proteins. Samples were reduced with 10 mM tris(2-carboxyethyl)phosphine (final concentration), incubated for 30 min at room temperature and then acidified to 0.5 M HCl. The samples were desalted using C18 96-well plates (3M Empore). The C18 eluates from homogenate samples were evaporated and stored at 4°C prior to MS analysis. The C18 eluates from light membrane and cytosol samples were collected in injection plates for strong cation exchange (SCX), dried by vacuum evaporation and stored at -20°C.
To fractionate peptides by SCX chromatography, samples were solubilized with reconstitution buffer (0.2% v/v formic acid, 10% v/v acetonitrile for light membrane samples; 20 mM K_2HPO_4, 25% v/v acetonitrile for cytosol samples) and loaded on an SCX column. Three fractions were collected following elution using a salt gradient. At the end of each SCX fractionation batch, the collected fractions were stored at -80°C. Once the SCX fractionation was completed, the fractions were freeze-dried and then desalted. The eluates were divided

equally into two 96-well plates; one plate for LC-MS/MS analysis and the other plate as a back-up. All plates were vacuum evaporated and stored at -20°C until analysis by LC-MS/MS. Samples were resuspended in 92.5/7.5 water/ACN+0.2% formic acid and analyzed by LC-MS/MS on a nanoAcquity UPLC (Waters) coupled to a Q-Exactive mass spectrometer (Thermo). Survey (LC-MS) and tandem mass spectrometry scans (MS/MS) were acquired in the same run. The resolution for the MS and MS/MS scans were 70,000 and 17,500, respectively. Peptide separation was achieved using a Waters nanoAcquity Symmetry UPLC Trap column (180 µm x 20 mm, 5 µm particle size) and a Waters nanoAcquity UPLC BEH300 analytical column (150 µm x 100 mm, 1.7 µm particle size). The mobile phases were (A) 0.2% formic acid in water and (B) 0.2% formic acid in acetonitrile. For each sample approximately 3.6 µg was loaded onto the trap column for 3 min at a flow rate of 10 µL/min. Peptides were separated using a linear gradient (92.5% A to 84% A) for 26 min, followed by a second one (84% A to 75% A) for 14 min and a wash at 60% B for 2 min. The flow rate was 1.8 µL/min. Protein identification was accomplished using data acquired by LC-MS/MS. The MS/MS spectra were matched to the corresponding peptide sequences found in the UniProt human protein database using Mascot (Matrix Science, version 2.2.06.) software.

2.6. Multiplexed multiple reaction monitoring (MRM) assay

For each of the selected proteins, five MRM-suitable peptides were selected by CellCarta's in-house MRM Peptide Selection software. If possible, peptides that were detected by mass spectrometry were prioritized. The selected peptides were synthesized by JPT Peptide Technologies (Germany). Synthesized peptides were resolubilized in 25%/75% water/DMSO (v/v), pooled and diluted with 0.2% formic acid in water to a concentration of 200 pmol/mL. This peptide mix was used to develop the MRM assay. The optimal 2 transitions (combination of peptide precursor and fragment ion mass-to-charge ratio that are monitored by the mass spectrometer) per peptide were determined using selected reaction monitoring (SRM)-triggered MS/MS on a QTRAP 5500 instrument (AB Sciex) coupled to a nanoAcquity UPLC (Waters). An SRM transition was predicted for each peptide. The detection of this transition triggered the acquisition of a full MS/MS spectrum of the target peptide. The two most intense fragment ions (b or y fragment ions only) in the MS/MS spectrum for each acquired peptide were recorded by in-house developed software. The mass spectrometer collision energy (CE) was optimized for each transition with 5 different CE values automatically generated by in-house developed software. A solution containing all synthesized peptides at a concentration of 200 pmoL/mL was analyzed with the created MRM method. The two best peptides per proteins were selected to be monitored by the MRM assay.

The processed samples were resolubilized with 11 µL of a reconstitution solution containing 5 internal standard (IS) peptides each at 100 ng/mL. Eight (8) µL of material (~10 µg) was analyzed by LC/MRM-MS. Peptide separation was achieved using a BioBasic C18 column (Thermo) (320 µm x 150 mm, 5 µm particle size). The mobile phases were (A) 0.2% formic acid in water and (B) 0.2% formic acid in acetonitrile. Peptides were separated using a linear gradient (92.5% A to 60% A) for 21 min, followed by a wash at 60% B for 2 min. The flow rate was 10 µL/min. The transition peak areas were integrated using Elucidator software

(Rosetta Biosciences) in combination with software developed at CellCarta for automated MRM peak integration.

2.7. Data processing and statistical analysis

For the analysis of the carbon fiber amperometry, data was first standardized (mean=0 and variance=1). Data was then normalized by quantile method using *preprocessCore* R package. PCA analysis was performed using *FactoMineR and factoextra* R packages. For comparison between tumor and non-tumor cells, non-paired Wilcoxon test was performed.

For the differential expression analysis by mass spectrometry, the intensity values for all detected components were log (base e) transformed with values < 0 replaced by 0. Intensity data was normalized to account for small differences in protein concentration between samples. A subset of the samples was used to create a reference sample against which all samples were then normalized. The normalization factors were chosen so that the median of log ratios between each sample and the reference sample over all the peptides was adjusted to zero. Intensities below Limit of Detection (LOD=100000) after normalization, were then linearly mapped to the range of (LOD/2, LOD) to avoid spurious large fold changes. Intensities above LOD were not changed. A two-way ANOVA model was used for the peptide level analysis and is defined as follows: $I_{ijk}=M+C_i+S_j+\varepsilon_{ijk}$ where I is the peptide intensity, M is the overall average intensity, C the 'clinical group' factor (matched non-tumor and tumor), S the 'patient' factor that takes into consideration the 'pairing' nature of the data, and ε random error. FDR (False Discovery Rate) and q-value were calculated, based on the p-values obtained from the ANOVA model, using the Storey Tibshirani method to make multiple testing adjustments. Tukey's HSD (Honestly Significant Difference) method was used to perform post hoc contrast among different groups.

One protein may have several identified and quantified peptides. The following ANOVA model, which is an extension of the two-way ANOVA used above in the peptide level analysis, takes this into consideration by introducing a 'peptide factor' in the model: $I_{ijkl}=M+C_i+S_j+P_k+\varepsilon_{ijkl}$ where I is the protein intensity, M an overall constant, C the 'clinical group', S the 'patient' factor, and P the peptide factor. The number of the levels for P is protein-dependent, equal to the number of identified and quantified peptides for the protein.

For Multiple reaction monitoring (MRM) analysis, differential intensity (DI) ratios were calculated in pair wise comparisons for each transition as the median of the ratio of the normalized intensities of each group. Paired Student's t-test was applied for the expression analysis. Protein-level statistics were also computed by linearly combining the transitions of a given protein into a single variable and then a t-test was applied.

All differential expression analysis and data visualization were done using R. PCA analysis was done using *prcomp* function from stats R package and plotted using ggplot2 R package. Volcano plot was performed using *EnhancedVolcano* function from R package.

2.8. Transcriptomic analyses

Gene expression data were retrieved from the GSE19422 dataset (https://www.ncbi.nlm.nih.gov/geo/query/acc.cgi?acc=GSE19422) [23] which includes 6

normal adrenal medulla and 61 Pheos. Consistently with the proteomic analysis, the 23 paraganglioma samples were not considered. The GSM483021 Pheo sample was excluded from our analysis because its transcriptomic profile, as revealed by clustering and UMAP analyses (data not shown), was similar to that of normal samples, suggesting that it was misidentified. The expression level of each gene was calculated as the geometric mean of the significantly differentially expressed probes identified with the GEO2R web tool using a Benjamin-Hochberg FDR correction (q-values < 0.05). Genes of the regulated exocytosis (#BPGO:0045055), secretory granule (#CCGO:0030141), catecholamine biosynthetic process (#GO:0042423), monoamine transport (#GO:0008504) and dopamine catabolic process (#GO:0042420) GO terms were then selected for further analysis. Unsupervised hierarchical clustering was performed with Bioconductor (v.3.13) and R software (v.4.1.0) using Pearson correlation as distance calculation and complete linkage. The Fold Change (FC) for each gene was calculated from the median expression values for the normal and Pheo groups and only those with a FC greater than or equal to 2 were retained for further analysis.

The correlation between the expression level of common genes and proteins was evaluated in both cytosolic and membrane fractions using Spearman correlation (GraphPad Prism v.8.1). In order to highlight functional clusters, an integrative analysis was conducted with Cytoscape software (v.3.8.2, [24]) using expression data and protein interaction data retrieved from STRING-DB (https://string-db.org, [25]). An edge-weighted force directed layout has been applied to the interaction network. Gene/protein clusters were identified using the CytoCluster plugin for Cytoscape using the default settings except for minimum size: 6, Minimum density: 0.25, Edge weights: combined score, Node penalty:1.

3. Results

3.1. Technical workflow and overall patient characteristics

This study includes two types of analyses (see technical workflow in Figure 1) performed on histologically confirmed Pheo samples from 27 distinct patients. On one side, we have analyzed the secretory activity of single tumor cells. To do so, freshly resected Pheos originating from 22 patients were placed in primary culture in order to perform real-time single cell catecholamine secretion measurement using carbon fiber amperometry (Figure 1A). On the other side, we have used quantitative mass spectrometry analysis to measure the relative differential expression of proteins involved in the exocytic pathway in 5 other Pheo tissues, which were compared to the non-tumor adrenal tissues of the matched patient. To conduct this proteomic analysis, two subcellular fractions enriched for exocytic proteins (the cytosolic fraction and a low-density membrane fraction containing plasma membrane, Golgi, endosomes and secretory vesicles) were isolated from the pairs of matched tumor and non-tumor frozen tissues (Figure 1B).

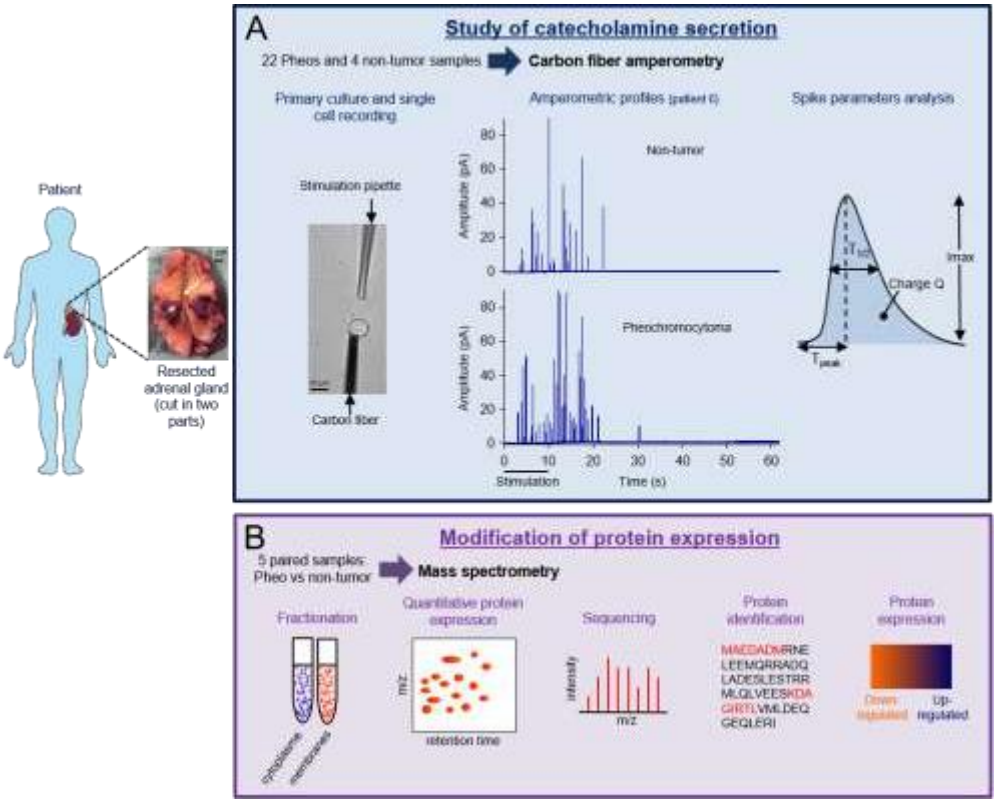

Figure 1: Technical workflow of catecholamine secretion measurement and comparative proteomic analysis of human Pheos. *Following total adrenalectomy, samples of Pheo (asterisk) and of non-tumor tissue (arrow) are collected and placed in culture for carbon fiber amperometry analysis (A) or proceeded for subcellular fractionation and mass spectrometry analysis (B). (A) Description of the different steps of the catecholamine secretion measurement by carbon fiber amperometry. Image showing a carbon fiber affixed to a cultured Pheo cell along with the pipette containing the stimulation solution. Representative amperometric traces from a non-tumor cell and a Pheo cell are illustrated. The dark bar indicates when stimulation by 100 µM nicotine solution was applied. The parameters of individual spike that were analyzed are indicated. (B) Complete protein profiling workflow of differential mass spectrometry analysis between Pheo tissue and matched non-tumor tissue. Note that due to the low amount of tumor and non-tumor samples, it is technically impossible to perform both amperometry and mass spectrometry experiments on the same samples.*

For the 22 patients included in the amperometric analysis, a slight predominance of males was found (59%) and the mean age was 50.3 ± 10.6 years at diagnosis (Table 1). All patients in the study presented hormonal hypersecretion (100%), including adrenergic or noradrenergic phenotype in 14 (64%) and 8 (36%) cases, respectively. However, only 16 patients (73%) were diagnosed with hormonal-related symptoms, and 7 patients out of 16 tested (46%) were diagnosed with a genetic predisposition for Pheo (4 *NF1*, 1 *RET*, 1 *SDHB* and 1 *SDHD*). The mean tumor size was 4.5 cm (range 1.7-8 cm). Other biological and clinical characteristics are detailed in Table 1.

Biological and clinical characteristics of the 5 patients included for the proteomic analysis are detailed in Table 2. They presented a mean age of 57.8 ± 8.3 years, and all had hormonal-related symptoms at diagnosis, four of which being classified as adrenergic phenotype and one as noradrenergic phenotype. None of the patients had germline mutation (out of 3 patients tested). The mean tumor size was 4.9 cm (range 3-8 cm). Individual characteristics of the 27 patients can be found in Supplementary Table 1.

Table 1: Biological and clinical characteristics of the 22 patients from which Pheos were used for amperometric analysis.

Characteristics, *n available*	
Age at diagnosis: (mean ± SD, years), *n=22*	**50.3** ± **10.6**
Gender male/female: (%), *n=22*	**13/9** (59/41%)
Symptoms at diagnosis: *n=22*	
- Tumor-related symptoms (%)	**4** (18%)
- Hormonal-related symptoms (%)	**16** (73%)
Hormonal hypersecretion:	
- Adrenergic/noradrenergic phenotype, *n=22*	**14/8**
- Urinary MN, ULN ratio (mean ± SD), *n=19*	**9.3** ± **14.3**
- Urinary NMN, ULN ratio (mean ± SD), *n=19*	**7.7** ± **5.7**
- Plasma free MN, ULN ratio (mean ± SD), *n=15*	**4.5**± **5.1**
- Plasma free NMN, ULN ratio (mean ± SD), *n=15*	**6.1** ± **6.3**
- Plasma CGA, ULN ratio (mean ± SD), *n=12*	**3.3** ± **2.7**
Pathology:	
- Tumor size, cm (mean + range), *n=21*	**4.5** (1.7-8)
- Ki-67, % (mean + range), *n=12*	**2.0** (0-5)
- PASS (mean + range), *n=22*	**2.1** (0-6)
Genetics: *n=16*	
- No germline mutation (%)	**9** (56.25%)
- *NF1*	**4** (25%)
- *RET*	**1** (6.25%)
- *SDHB*	**1** (6.25%)
- *SDHD*	**1** (6.25%)

MN: metanephrine, NMN: normetanephrine, ULN: upper limit of normal range, CGA: chromogranin A, PASS: Pheochromocytoma of the Adrenal Gland Scaled Score, NF1: Neurofibromatosis type 1, RET: Rearranged during transfection, SDHB: Succinate dehydrogenase B, SDHD: Succinate dehydrogenase D.

Table 2: Biological and clinical characteristics of the 5 patients from which Pheos were used for proteomic analysis.

Characteristics, *n available*	
Age at diagnosis: (mean ± SD, years), *n=5*	**57.8** ± **8.3**
Gender male/female: (%), *n=5*	**2/3** (40/60%)
Symptoms at diagnosis: *n=5*	
- Tumor-related symptoms (%)	**1** (20%)
- Hormonal-related symptoms (%)	**5** (100%)
Hormonal hypersecretion:	
- Adrenergic/noradrenergic phenotype, *n=5*	**4/1**
- Urinary MN, ULN ratio (mean ± SD), *n=4*	**3.7** ± **4.2**
- Urinary NMN, ULN ratio (mean ± SD), *n=4*	**6.8** ± **8.0**
- Plasma free MN, ULN ratio (mean), *n=2*	**3.0**
- Plasma free NMN, ULN ratio (mean), *n=2*	**3.0**
- Plasma CGA, ULN ratio (mean), *n=2*	**4.7**
Pathology:	
- Tumor size, cm (mean + range), *n=5*	**4.9** (3-8)
- Ki-67, % (mean + range), *n=3*	**3.3** (1-7)
- PASS (mean + range), *n=3*	**3** (0-9)
Genetics: *n=3*	
- No germline mutation (%)	**3** (100%)

MN: metanephrine, NMN: normetanephrine, ULN: upper limit of normal range, CGA: chromogranin A, PASS: Pheochromocytoma of the Adrenal Gland Scaled Score.

3.2. Analysis of catecholamine secretion in human pheochromocytomas by carbon fiber amperometry

Representative amperometric traces recorded from a non-tumor cell and a Pheo cell were illustrated in Figure 1A. Each individual spike represents the release of catecholamine contained in a single granule and is composed of a rapid rise of the electrode current corresponding to the oxidation of catecholamines quickly released at high concentration through the fusion pore as it dilates. The spike rise is then followed by a slower decay representing a decreased of the catecholamine flux through the pore as the granule empties. In addition to the quantification of number of events per cell, the analysis of individual amperometric spikes provides valuable dynamic information on the exocytic process. Hence, the surface area or quantal size (Q) is proportional to the amount of catecholamine released per event, the spike amplitude value (Imax) reflects the maximal flux of catecholamines, whereas the half-width ($T_{1/2}$), and the time to peak (T_{peak}) reflect the duration of the exocytotic event and the kinetics of the fusion pore expansion, respectively (Figure 1A).

Primary culture of human Pheo cells is rather efficient as most attempts were successful. However, culturing non-tumor chromaffin cells taken outside the tumor zone appeared trickier and failed most of the time for unidentified reasons. Nevertheless, we were able to

obtain 4 different cultures of non-tumor cells that could be used for amperometric recordings. Therefore, we have compared the distribution of the amperometric parameters of each of the 22 patients individually with the median values calculated from these 4 non-tumor samples. All the amperometric parameters are detailed in Table 3. The major change concerns the total number of spikes per cell. Indeed, among the 22 patients, 16 (73%) exhibit a significant increase of the number of spikes per cell (11 patients with an increase up to 2-fold and 5 patients with an increase above 2 and up to 3.4-fold; Figure 2). Importantly, these data demonstrate that, upon the same stimulation, the content of a larger number of secretory granules is released in a Pheo cell compared to a non-tumor cell.

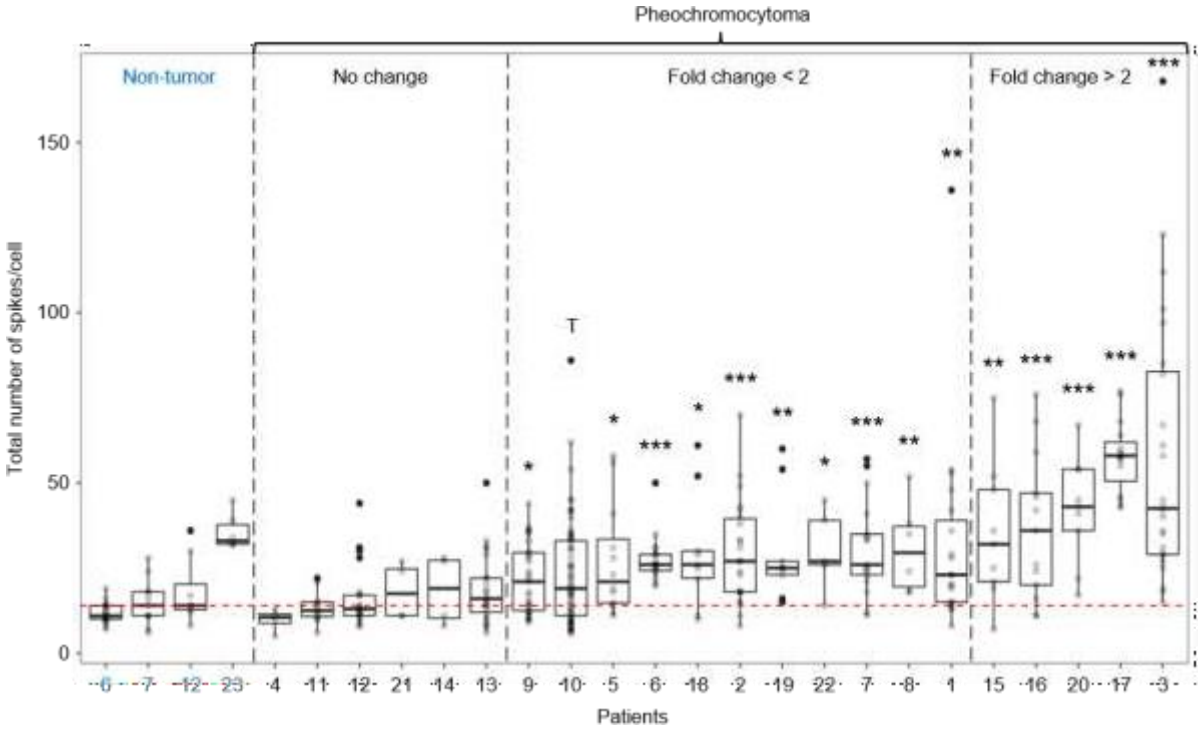

Figure 2: Analysis of catecholamine secretion events in Pheo cells from each patient by carbon fiber amperometry. *Box-and-whisker diagrams illustrating the distribution of the total number of amperometric spikes per cell for non-tumor cells and for cells from each patient with Pheo. Patients are classified according to the increasing effect of the total number of spikes per cell compared to the median of the non-tumor cells (n= 44 cells, pooled from the 4 non-tumor samples): no significant change, fold change < 2 and fold change > 2. The red dotted line indicates the median of non-tumor cells.* $^{T}p=0.05$, *$p<0.05$, **$p<0.01$, ***$p<0.001$ *compared to the median of all the non-tumor cells; non-paired Wilcoxon test.*

Table 3: Characteristics of amperometric spikes from 22 Pheos and 4 non-tumor tissues.

Identification	Number of cells	Total number of spikes	Total number of spikes/cell	Number of analyzed spikes	Imax (pA)	Charge (pC)	$T_{1/2}$ (ms)	T_{peak} (ms)
Non-tumor 6	19	224	11.79 ± 0.67	146	41.56 ± 2.23	2.22 ± 0.13	51.90 ± 1.14	42.21 ± 1.24
Non-tumor 7	11	164	14.91 ± 2.05	126	10.92 ± 0.81	0.92 ± 0.10	68.41 ± 3.41	29.87 ± 1.67
Non-tumor 12	8	144	18.00 ± 3.44	102	18.77 ± 2.35	0.73 ± 0.20	30.76 ± 3.94	13.50 ± 2.07
Non-tumor 23	6	214	35.67 ± 2.17	112	15.51 ± 1.65	0.97 ± 0.12	56.13 ± 4.26	28.50 ± 2.10
Patient 1	19	609	**32.05 ± 6.61 ****	469	21.34 ± 2.16	**0.90 ± 0.10 ***	**38.97 ± 2.70 *****	**16.37 ± 1.41 *****
Patient 2	22	653	**29.68 ± 3.26 *****	518	**12.45 ± 0.65 *****	**0.71 ± 0.04 *****	52.11 ± 1.69	**23.69 ± 1.03 *****
Patient 3	24	1388	**57.83 ± 8.01 *****	1032	27.85 ± 2.91	1.79 ± 0.16	**61.69 ± 2.74 ***	29.26 ± 1.42
Patient 4	4	39	9.75 ± 1.70	38	13.08 ± 3.20	0.71 ± 0.26	44.90 ± 8.53	21.05 ± 4.65
Patient 5	12	326	**27.17 ± 4.74 ***	240	**13.82 ± 0.92 ***	1.30 ± 0.11	**80.38 ± 5.65 *****	36.49 ± 2.11
Patient 6	18	499	**27.72 ± 1.60 *****	320	**45.78 ± 2.00 *****	**2.33 ± 0.10 *****	**48.34 ± 0.76 ***	40.43 ± 0.90
Patient 7	17	524	**30.82 ± 3.32 *****	408	**11.04 ± 0.58 ****	0.96 ± 0.07	**69.70 ± 3.27 ****	30.43 ± 1.43
Patient 8	6	185	**30.83 ± 5.46 ****	163	30.99 ± 4.50	2.00 ± 0.29	65.30 ± 6.54	31.31 ± 2.67
Patient 9	31	682	**22.00 ± 1.85 ***	416	**40.28 ± 1.61 *****	1.71 ± 0.08	**40.29 ± 1.13 *****	34.45 ± 1.18
Patient 10	59	1382	**23.42 ± 2.04 ^{T}**	1231	21.26 ± 1.28	1.25 ± 0.08	52.81 ± 2.19	**26.49 ± 1.06 ****
Patient 11	12	161	13.42 ± 1.31	130	17.39 ± 2.35	**0.85 ± 0.11 ***	**42.54 ± 2.76 ***	**19.00 ± 1.75 *****
Patient 12	21	345	16.43 ± 2.01	292	20.17 ± 2.71	**0.81 ± 0.10 ****	**35.45 ± 1.20 *****	**16.75 ± 0.84 *****
Patient 13	23	428	18.61 ± 2.16	353	**11.28 ± 0.81 *****	**0.68 ± 0.05 *****	52.01 ± 2.47	**25.47 ± 1.13 ****
Patient 14	4	74	18.50 ± 5.24	59	27.09 ± 5.68	1.01 ± 0.14	**35.08 ± 1.80 ***	**16.11 ± 0.79 ***
Patient 15	9	315	**35.00 ± 6.88 ****	187	**13.91 ± 1.93 ***	**0.49 ± 0.08 *****	**30.03 ± 1.99 *****	**14.59 ± 1.13 *****
Patient 16	12	482	**37.08 ± 5.96 *****	334	21.58 ± 2.30	**0.93 ± 0.14 ***	**37.39 ± 2.83 ****	**20.30 ± 3.34 ****
Patient 17	15	866	**57.73 ± 2.76 *****	400	23.72 ± 1.15	1.04 ± 0.06	**39.65 ± 0.89 *****	30.66 ± 0.84
Patient 18	9	266	**29.56 ± 5.66 ***	140	19.18 ± 1.75	1.72 ± 0.24	**79.57 ± 6.60 *****	**41.97 ± 4.35 ***
Patient 19	9	270	**30.00 ± 5.31 ****	197	**13.96 ± 1.03 ***	**0.55 ± 0.04 *****	**35.21 ± 1.19 *****	**17.32 ± 0.74 *****
Patient 20	9	379	**42.11 ± 5.25 *****	276	15.84 ± 2.19	**0.60 ± 0.10 *****	**33.53 ± 2.29 *****	**16.95 ± 1.58 *****
Patient 21	4	73	18.25 ± 4.23	59	16.29 ± 5.83	0.74 ± 0.19	45.37 ± 2.51	22.65 ± 1.94
Patient 22	5	151	**30.20 ± 5.42 ***	82	25.13 ± 5.40	1.72 ± 0.30	65.82 ± 6.82	32.50 ± 3.74

*Amperometric recordings were performed on primary culture of human Pheo cells or non-tumor cells. Cells were stimulated with 100 µM of nicotine for 10 s. The number of cells, the total number of amperometric spikes per cell and the different amperometric spikes parameters are indicated. Results represent the mean ± SEM. Bold values are considered significantly different from the non-tumor condition; $^{T}p=0.05$, *p< 0.05, **p< 0.01, ***p< 0.001 compared to the median of non-tumor cells; non-paired Wilcoxon test.*

To better understand which parameters were mostly driving the secretory profiles of tumors and to sort out potential patient clusters, we performed a principal component analysis (PCA) using the amperometric data obtained from the 22 tumor cell cultures (Figure 3). As shown in Figure 3A, the 3 first principal components explain all the data variations (97.3%). The correlation matrix indicated that the main amperometric parameters explaining the variation of the data within the 2 first dimensions are the charge (Q) and the T_{peak} and to a lesser extend the $T_{1/2}$, parameters that are all correlated as shown by the variable projection analysis. The total number of spikes per cell are less correlated and largely contributes to the third PCA dimension. Thus, it is interesting to note that the distribution of the patient samples plotted according to the first and the third component reveals a clear separation between populations with and without exocytic event increase as compared to non-tumor cells (Figure 3B). The distribution of the patient samples plotted according to the two first components forms one major cluster including most of the patients for which the two kinetic parameters, $T_{1/2}$ and T_{peak}, are significantly decreased (Figure 3C). Indeed, in 14 (64%) tumors, cell cultures presented a significant reduction of the $T_{1/2}$ and/or T_{peak}, often accompanied (9 patients) with a slight reduction of the quantal size (Charge Q; Figure 4A, B and Table 3). This type of amperometric profile corresponds to exocytic events occurring with a faster kinetics compared to non-tumor cells. Interestingly, among these 14 patient samples, 10 displayed a concomitant increase of the total number of spikes per cell (Figure 2).
On the contrary, only 4 patients' cultured cells (18%) displayed, a significant increase of their $T_{1/2}$ leading, for 2 patients, to a reduce spike amplitude (Imax, patients 5 and 7, Figure 4C and Table 3) and accordingly to a slower release kinetics. Four patients' cultured cells (18%) do not show significant changes in charge, $T_{1/2}$ or T_{peak} indicating that the kinetic of the secretion is unaffected (Figure 4D). Finally, it is interesting to note also that the quantal size of the spikes remained unchanged or slightly decreased for 21 patients indicating that the level of catecholamines per secretory granules does not increase in Pheo cells.

Altogether, our analysis of the amperometric recordings indicate that catecholamine secretion in tumor cells from patients with Pheo is increased because it involves a higher number of fusion events per stimulation compared to non-tumor cells. Moreover, in addition to being more numerous, the exocytic events are faster in tumor cells, which may contribute to recruit more granules upon similar stimulation.

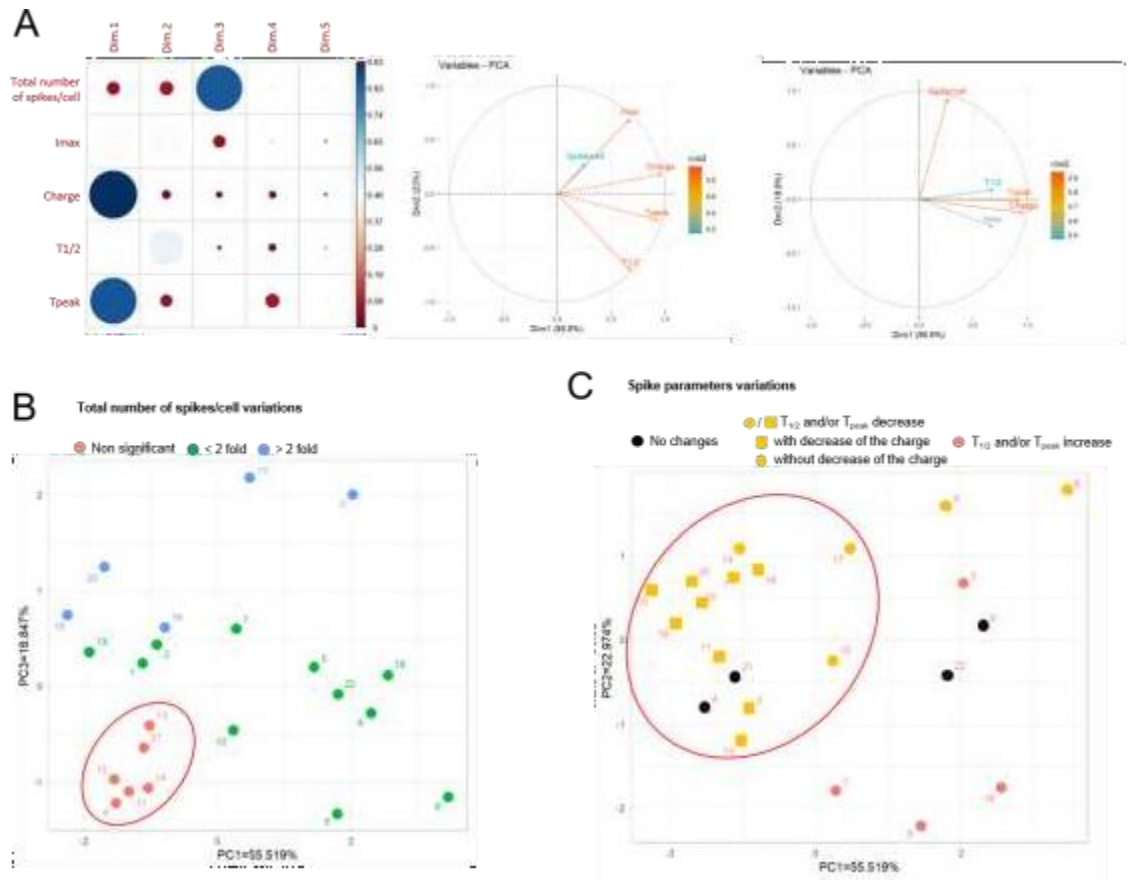

Figure 3: Principal component analysis (PCA) of amperometric spike parameters corresponding to catecholamine secretion recordings on tumor cells cultured from 22 patients with Pheo. *Total number of spikes/cell and spike parameters (Imax, Charge, $T_{1/2}$ and T_{peak}) were subjected to PCA. (A) Correlation matrix and variable factor maps along the PCA dimensions. The first, second and third dimension (Dim) of principal components explain 55.5%, 23.0% and 18.8% of the data variations, respectively. The spike parameters Charge and T_{peak} largely contribute to Dim1, whereas $T_{1/2}$ and total number of spikes per cell contribute to Dim2 and 3, respectively. PCA variable vector map showing the projection of Imax, Charge, T_{peak} and $T_{1/2}$ on Dim2 (right) and Dim3 (left). The projection of each variable vector gives an indication of the relation of these variables to T_{peak} and Charge (Dim1) or total number of spikes/cell (Dim3). (B-C) The two-dimensional representation of PC1 and PC3 (B) allowed to separate patients according to the significant variation of the total number of spikes recorded per cell (red circle = no change; green circles = fold change < 2; blue circles = fold change > 2). The two-dimensional representation of PC1 and PC2 (C) revealed a large cluster of patients for which $T_{1/2}$ and/or T_{peak} decreased (yellow squares and circles).*

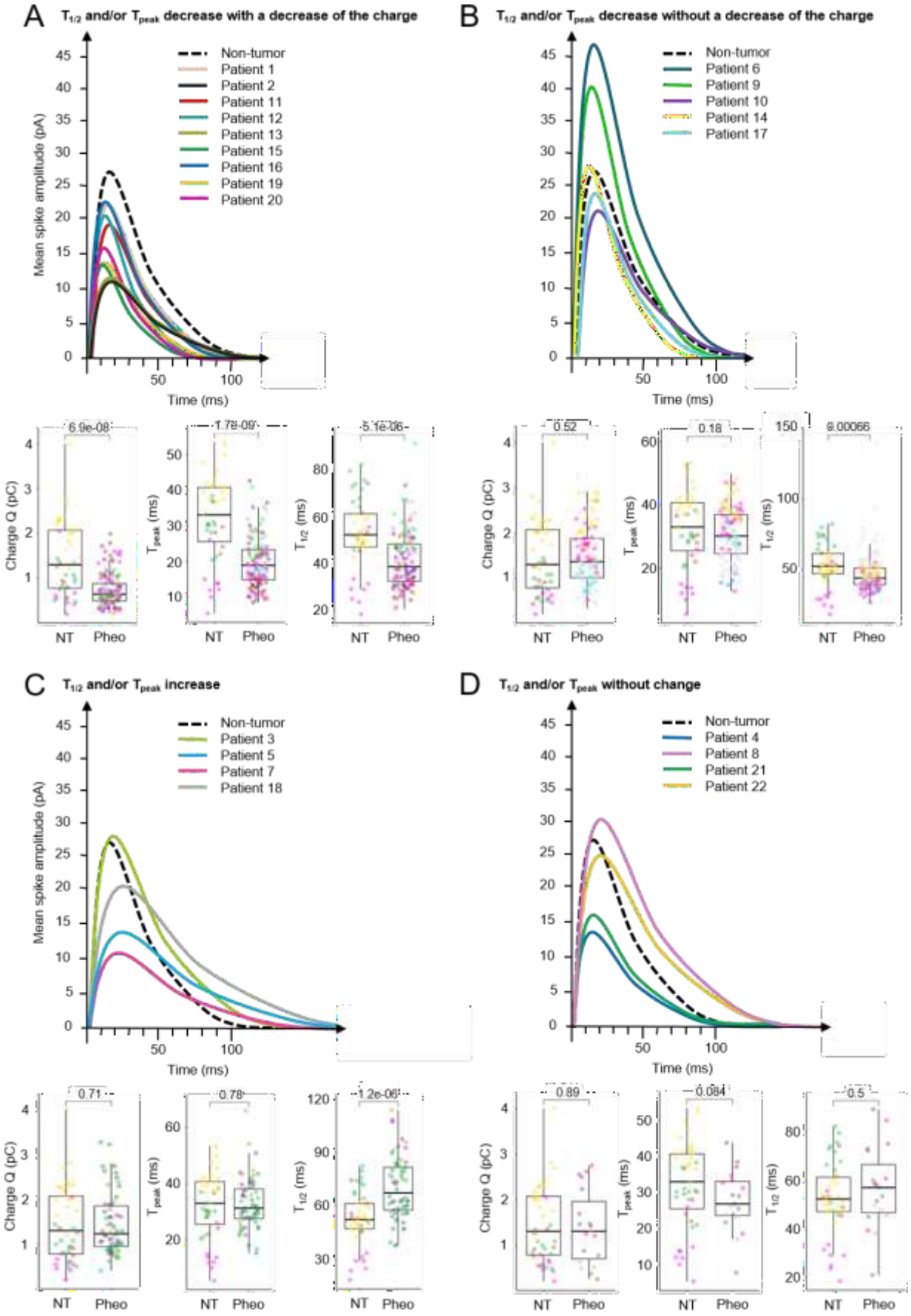
A
T1/2 and/or Tpeak decrease with a decrease of the charge
Non-tumor
Patient 1
Patient 2
Patient 11
Patient 12
Patient 13
Patient 15
Patient 16
Patient 19
Patient 20
Mean spike amplitude (pA)
Time (ms)
B
T1/2 and/or Tpeak decrease without a decrease of the charge
Non-tumor
Patient 6
Patient 9
Patient 10
Patient 14
Patient 17
Time (ms)
6.9e-08
1.7e-09
5.1e-06
0.52
0.18
0.00066
Charge Q (pC)
Tpeak (ms)
T1/2 (ms)
NT
Pheo
C
T1/2 and/or Tpeak increase
Non-tumor
Patient 3
Patient 5
Patient 7
Patient 18
Mean spike amplitude (pA)
Time (ms)
D
T1/2 and/or Tpeak without change
Non-tumor
Patient 4
Patient 8
Patient 21
Patient 22
Time (ms)
0.71
0.78
1.2e-06
0.89
0.084
0.5
Charge Q (pC)
Tpeak (ms)
T1/2 (ms)
NT
Pheo

Figure 4: Analysis of amperometric spike parameters in each patient's cells. *Superimposition of the averaged spike obtained from Pheo and non-tumor (NT) cells of each patient and distribution of the values corresponding to the spike charge (Q), the spike rise time (T_{peak}) and the spike half-width ($T_{1/2}$) are shown for the 4 different populations of patients: (A) decrease of $T_{1/2}$ and/or T_{peak} with lower charge, (B) decrease of $T_{1/2}$ and/or T_{peak} without lower charge, (C) increase of $T_{1/2}$ and/or T_{peak} and (D) no significant change of $T_{1/2}$ and/or T_{peak}. Box- and-whisker diagrams illustrate the distribution of each variable values pooled from all the patients belonging to the indicated secretory profile. P values are indicated and patients are color coded. All the average amperometric data are detailed in Table 3.*

3.3. Differential protein expression of the exocytic machinery in human pheochromocytomas

Since catecholamine release is altered in Pheos, we asked whether proteins of the core machinery of secretory granule exocytic process could be deregulated. To do so, we performed a mass spectrometry analysis comparing 5 pairs consisting of human Pheos with their respective matched adjacent non-tumor tissues. To increase detection and sensitivity, we conducted the proteomic analysis on purified subcellular fractions in place of total homogenate. Two main subcellular fractions were isolated from each tissue sample, a membrane fraction enriched for organelles and vesicles derived from the exocytic pathway and a fraction enriched in cytosolic proteins. From our proteomic dataset, we selected proteins from the regulated exocytosis (#BPGO:0045055) and secretory granule (#CCGO:0030141) GO terms. Moreover, as expression level of proteins involved in catecholamine synthesis, storage and catabolism are known to impact the amount of catecholamines in Pheos, we have also included proteins from the catecholamine biosynthetic process (#GO:0042423), monoamine transport (#GO:0008504) and dopamine catabolic process (#GO:0042420) GO terms. We focused on proteins significantly up or downregulated in the tumor tissue by comparison with the corresponding non-tumor tissue, with fold change values greater than or equal to 2.

In these conditions, we identified 175 deregulated proteins: 63 proteins from the cytosolic fraction, 59 from the membranes-enriched fraction and 53 common to both fractions (Figure 5A). Supplementary Table 2 details the median value of the relative expression changes of the 5 Pheos in comparison with their matched non-tumor tissues for all these 175 selected proteins, associated with their known function in exocytosis. The volcano plots in Figure 5B shows the relationship between the p-values and the fold change in expression for proteins detected in the cytosol or in membranes-enriched fractions. The unsupervised hierarchical clustering of all differentially expressed proteins in row according to the paired samples in columns, is presented in Figure 5C for the corresponding cellular compartment. Note that the expression of proteins found in common in the membranous and the cytosolic fractions varies in the same direction (Supplementary Figure 1). This specific dataset of proteins corresponding to the proteins involved in the machinery of secretory granule exocytotic process and in catecholamine metabolism clearly differentiates, by their modulation of expressions, the Pheo samples from the non-tumor samples. The functions of the deregulated proteins linked to secretory granule exocytosis include mainly: secretory granule organization and biogenesis, hormone processing and catecholamine metabolism, vesicular trafficking, docking, priming, membrane fusion, actin cytoskeleton organization, and small GTPases

(Supplementary Table 2 and Figure 5D). Hence, we observed that numerous secretory granule cargos, enzymes involved in the catecholamine metabolism as well as different proteins involved in the control of the frequency and the dynamic of the exocytic events are up-regulated.

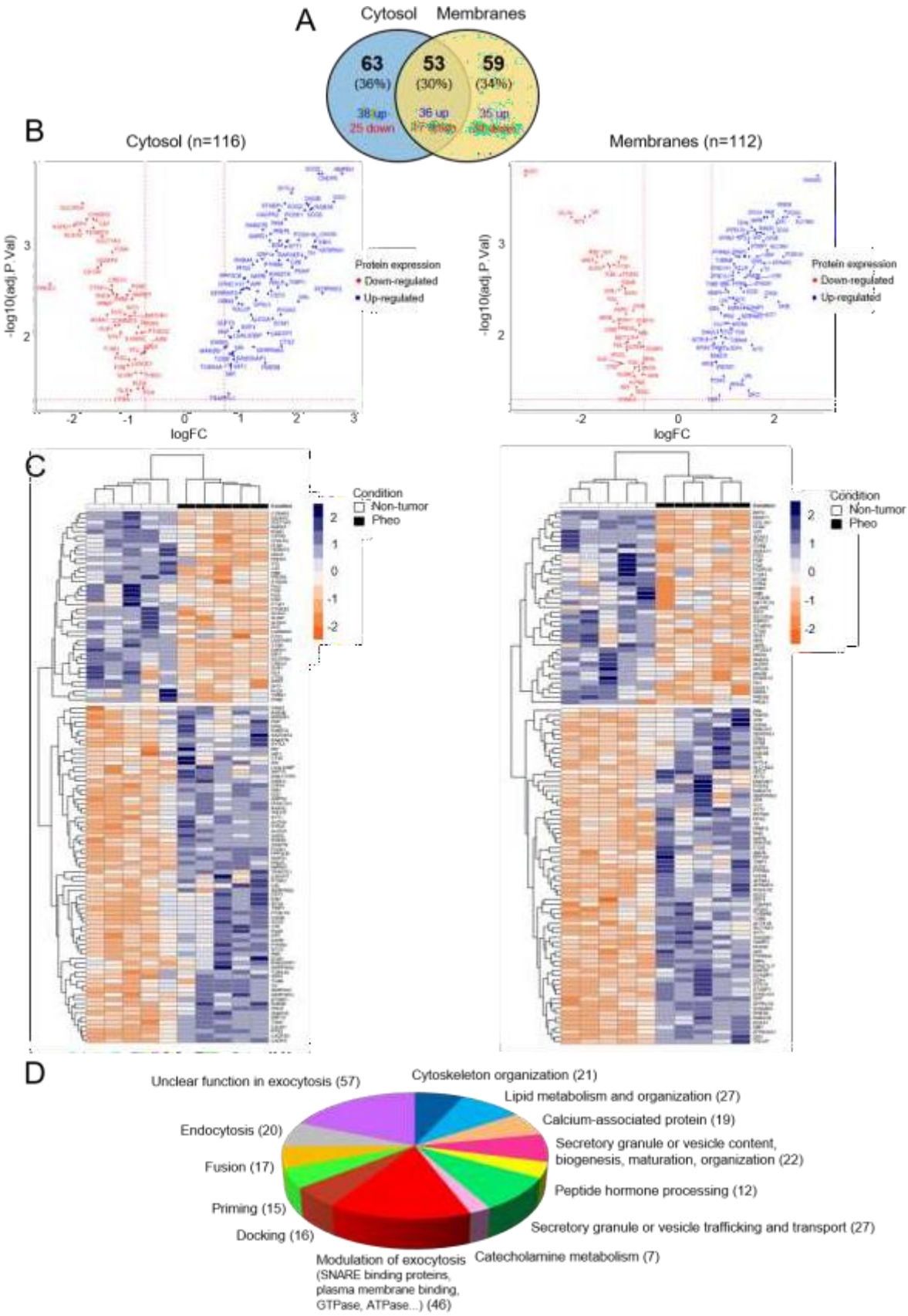

Figure 5: Identification of differentially expressed proteins involved in the exocytotic pathway in human Pheo tissues. *(A) Venn diagram showing the distribution of the differentially expressed*

proteins in fractions enriched in cytosolic and membrane proteins. Colors indicate up- (blue) or down- (red) regulation. (B) Volcano plots of all differentially expressed proteins between Pheos and non-tumor samples, FC: fold change. (C) Two-way hierarchical clustering of paired samples from each patient (non-tumor in white and Pheo in black) in column according to the validated cytosolic (left) and membranous (right) proteins of the dataset in row. Protein expression values were z-score normalized prior to clustering using the complete-linkage method together with the Euclidean distance. Each row represents a differentially expressed protein and each column a patient according to the tissue type. The color scale illustrates the relative level of protein expression: blue, higher expression; red, lower expression. (D) Functional enrichment analysis of identified proteins. Each differentially expressed protein selected for their potential role in exocytosis (Supplementary Table 2) has been classified in one or several indicated biological functions. The number of proteins in each function is indicated in parenthesis.

To further assess the relevance of our data, we have compared our proteome dataset to a published gene expression analysis of 60 Pheos and 6 normal adrenal medulla tissues ([23] https://www.ncbi.nlm.nih.gov/geo/query/acc.cgi?acc=GSE19422). Using this analysis, we have extracted 183 genes that belong at least to one of the 5 GO terms used in the proteomic analysis and that are significantly differentially expressed by at least two-fold between Pheos and normal adrenal tissues. Interestingly, among these 183 genes, 64 are common to our proteome dataset. As observed at the level of the protein expression changes, the hierarchical clustering of these 64 differentially expressed genes efficiently separated the tumor samples from the normal adrenal tissues (Figure 6A). Moreover, the expression of 58 of these 64 genes (91%) shows the same variation trend as the protein expression, both in the cytosol and in the membranes (Figures 6B, C and Supplementary Figure 2). To visualize whether the deregulated proteins identified in this comparison were highly connected to each other, we performed a protein-protein interaction (PPI) network analysis using Cytoscape ([24]**,** Figure 7). Interestingly, one major significant cluster is composed of proteins that are overexpressed both at the protein and at the gene levels (blue squares). The cluster includes proteins involved in the secretory granule composition such as various chromogranins (CHGA, CHGB, SCG2, SCG3, SCG5), in catecholamine metabolism (TH, DDC, DBH), monoamine vesicular transport (VMAT/SLC18A-1 and 2) or hormone processing (PCSK1, PCSK2, CPE, PAM), in granule docking and fusion such as different SNAREs or SNAREs interacting proteins (SNAP25, STX1A, STXBP1, SYT1) and Rab GTPases (RAB3A, RAB3D, RAB27B).

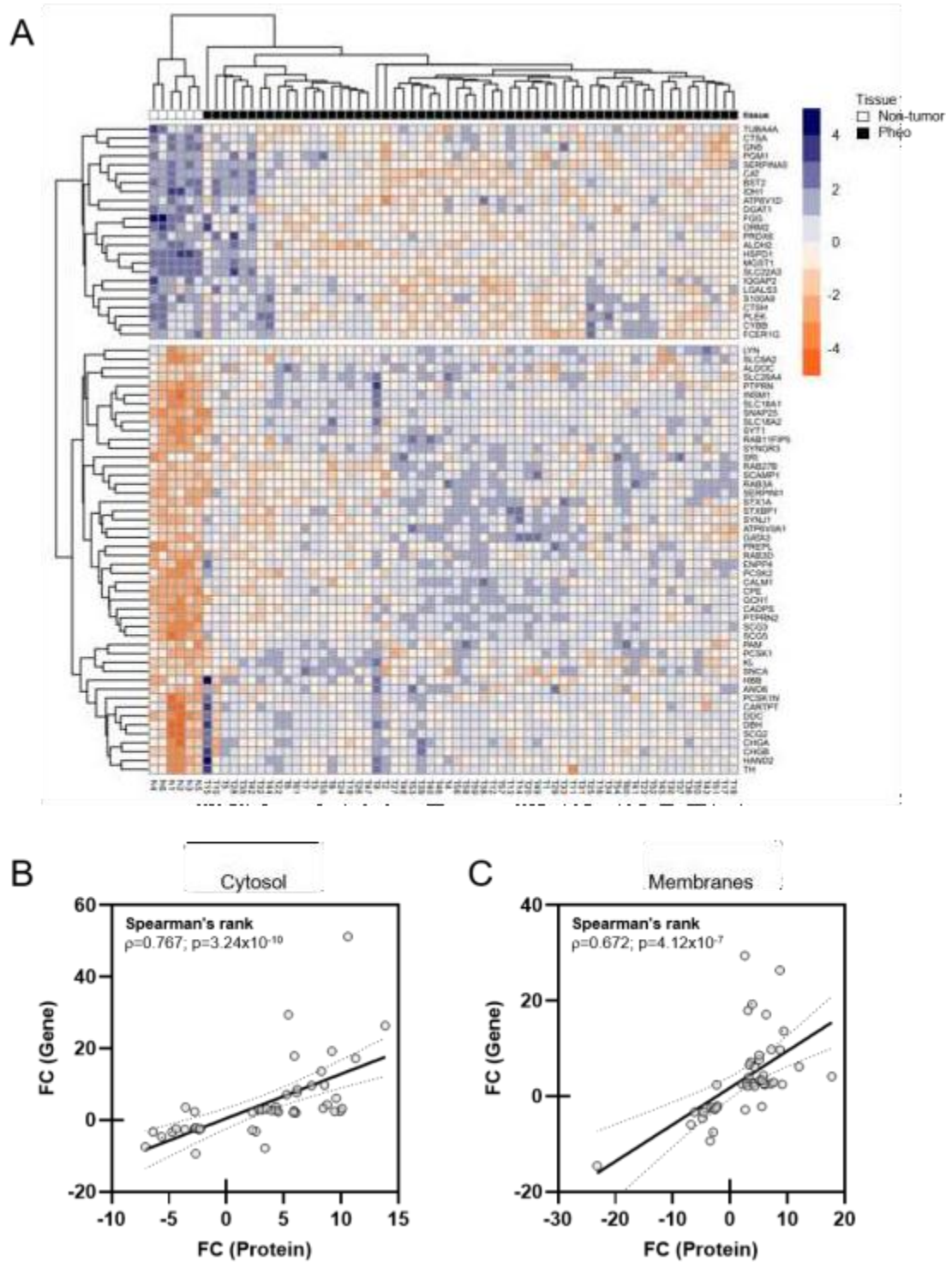

Figure 6: Comparison of the proteome dataset with a published gene expression analysis of 60 Pheos and 6 normal adrenal medulla tissues. *(A) Unsupervised hierarchical clustering of selected gene expression profiles (n=64) for 6 non-tumor adrenal medulla (in white) and 60 Pheo (in black) tissues from Lopez-Jimenez et al. (2010). The color scale illustrates the relative level of gene expression: blue, highly expressed gene; red, low expressed gene. (B-C) A significant positive correlation was evidenced between the fold change (FC) of genes and corresponding cytosolic (B;* $\rho=0.767$, $p=3.24x10^{-10}$*) or membrane (C;* $\rho=0.672$, $p=4.12x10^{-7}$*) proteins of the exocytosis pathway.*

Linear regression (solid line) and 95% confidence bands (the regions delineated by dotted lines) are shown in panels B and C.

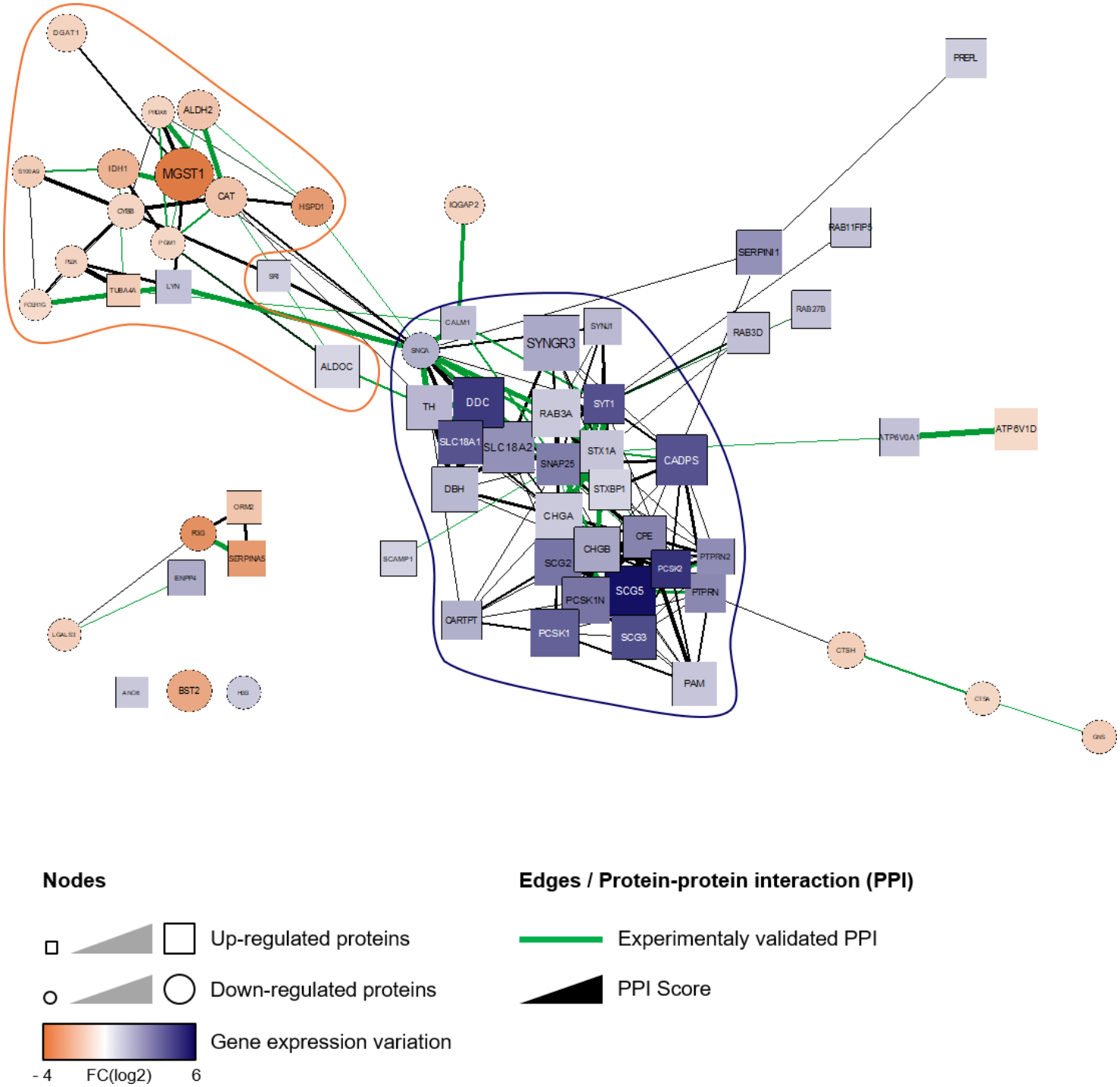

Nodes

Up-regulated proteins

Down-regulated proteins

Gene expression variation

- 4 FC(log2) 6

Edges / Protein-protein interaction (PPI)

Experimentaly validated PPI

PPI Score

Figure 7: Protein-protein interaction (PPI) network analysis of the exocytic proteins modulated in Pheos at the transcriptomic and protein level. *The PPI network was generated using Cytoscape. Up- and down-regulated proteins are represented by square and round nodes, respectively and the level of protein expression is proportional to their size whereas the mRNA expression variation is color coded as indicated. Therefore, blue squares and red circles represent candidates for which both protein and mRNA are overexpressed or downregulated, respectively. The 2 first clusters identified by the*

CytoCluster plugin are outlined in blue ($p>10^{-9}$) and red ($p=3.01x10^{-6}$). Note that the variation observed at the protein and mRNA level goes in the same direction for 58 proteins out of 64 (91%), FC: fold change.

Finally, to further validate our dataset, we analyzed the global expression change of few key overexpressed proteins (17) selected from our proteomic dataset. To do so, we performed a multiplexed MRM-MS assay in total protein homogenates prepared from another independent cohort of 25 pairs of human Pheos and their matched non-tumor tissues [26]. As MRM is a targeted MS approach that uses synthetic peptide reference standards, it is used to confirm and quantify the presence of proteins of interest on smaller amounts of sample with high sensitivity, which eliminates the need for fractionation [27]. As observed for the subcellular fractions, using MRM-MS we found that the expression of the 17 selected proteins was also significantly increased in Pheos compared with the matched adjacent non-tumor tissues (Figure 8).

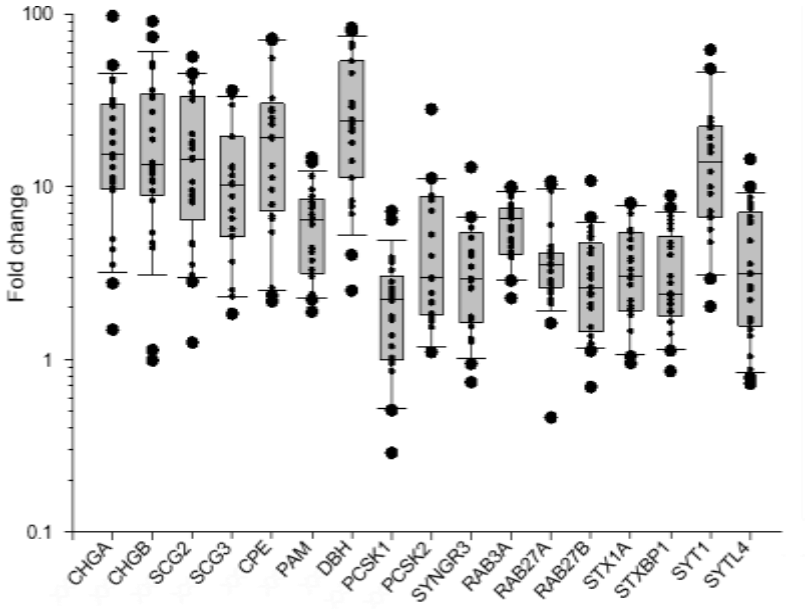

Figure 8: Global variation of key exocytic proteins expression in human Pheo tissues. *Expression variation of the indicated proteins was quantified at the protein level by MRM-MS in 25 Pheos normalized to their matched adjacent non-tumor tissues. Box- and-whisker diagrams illustrate the distribution of protein expression fold change for the 25 Pheos.*

4. Discussion

Dysfunction of hormones and neuropeptides secretion in NETs is a serious health issue. Patients with midgut primary carcinoids have increased serotonin and metabolite secretion, corresponding to higher metastatic tumor burdens [28]. Hypersecretion of serotonin by carcinoid tumor from the gastro-intestinal tract can trigger carcinoid syndrome, which is associated with severe consequences such as flushing, diarrhea, bronchoconstriction and cardiac valvular disease [28]. Acromegaly often result from excessive secretion of growth hormone by pituitary adenoma [29]. Excessive level of circulating catecholamines in patients with Pheo can trigger life-threatening medical problems such as cardiomyopathies and stroke [11, 30]. Moreover, enhanced secretory activity of NET cells may develop over time with negative impact on prognosis. For example, silent pituitary adenoma can evolve into an active secreting adenoma whereas non-functional pancreatic tumor can become hormonally active, hence turning to a more aggressive tumor phenotype [31-33]. Small cell lung cancer (SCLC) is a high-grade malignant cancer due to the progressive neuroendocrine nature of SCLC cells that secrete a variety of neuropeptides, together with growth factors that all dramatically accelerate the invasive growth by their autocrine action [34, 35]. Altogether, these few examples taken from a longer list clearly reveal that dysfunction of the secretory pathways in NETs can lead to severe clinical complications and can also impact the tumor development and prognosis. Today, a clear yet unmet need is to identify the cellular and molecular mechanisms triggering hypersecretory activity in NETs.

The aim of the present study was to uncover part of the mechanisms triggering catecholamine hypersecretion in human Pheo cells. To do so, we have used carbon fiber amperometry recordings to analyze catecholamine secretion on individual tumor cells cultured directly from freshly resected human Pheos. In parallel, we have analyzed the expression level of various proteins involved in calcium-regulated exocytosis by differential mass spectrometry methods applied on human Pheo tissues.

Numerous studies reported the up-regulation of mRNA or proteins controlling catecholamine synthesis leading to an increased level of catecholamines in Pheo tissues [36-40]. In agreement, we have found here by mass spectrometry that TH, DDC and DBH are significantly overexpressed in Pheos. How the excess of catecholamines is regulated at the cellular level remains an intriguing question. Subcellular catecholamine storage in chromaffin cells depends on a dynamic equilibrium between the active transport in the granule by the vesicular monoamine transporters (VMAT) and the passive leakage through the granular bilayer towards the cytoplasm. At the equilibrium, catecholamines remaining in the cytoplasm are either deaminated by the monoamine oxidase (MAO) or transformed in metanephrines by the catechol-O-methyltransferase (COMT; for a review see [41]). Accordingly, we also observed a large increase of the vesicular monoamine transporters VMAT1 and 2 expression level in Pheo tissues,

whereas MAO1 and 2 were downregulated, the latter favoring the increase of cellular metanephrines synthesis by COMT [38, 42, 43]. However, it remained unclear to us whether increasing the number of copy of VMAT at the surface of a single granule will necessarily increase its catecholamine content.

Here we have analyzed one by one a total of 7344 individual amperometric spikes from Pheo cells. One amperometric spike represents the release of a single secretory granule and the spike quantal size (charge; Q) is directly proportional to the amount of catecholamines contained within this granule [13, 22]. Note that it is unlikely that part of the overexpressed monoamine transporters would be miss-targeted to the vesicles involved in constitutive exocytosis as we never observed any spontaneous amperometric spike in the absence of cell stimulation (data not shown). Interestingly, we observed that the average spike charge in Pheo cells did not increase compared to non-tumor cells, and it even slightly decreased for 9 tumors. These results suggest that each single secretory granule in Pheo cells does not contain more catecholamines than in non-tumor cells. In consequence, the best hypothesis to link an excessive cellular catecholamine production with a higher expression of monoamine transporters (along with others granular proteins), but without enhanced granule filling would be an overall increase of the number of secretory granules in Pheo cells. Accordingly, various specific soluble cargos of secretory granules, like different chromogranins or enzymes involved in hormone processing or granule biogenesis, were also found to be overexpressed (Figure 5D and Supplementary Table 2), in line with previous reports indicating that chromogranins or chromogranin-derived peptides are highly expressed in Pheo [44]. Probing this hypothesis requires however, further investigations and we have started to collect new human samples to address this question in the future through electron microscopy imaging.

Importantly, our analysis by carbon fiber amperometry allowed us to demonstrate that the total number of spikes per cell is significantly increased in Pheo cells compared to non-tumor cells. It indicates that, upon similar stimulation, more exocytic events occurs, which led to more catecholamine secretion at the single cell level. Moreover, by analyzing the spike kinetics, we have also observed that, for many patients, these exocytic events tend to be faster. Altogether, these data demonstrated that calcium-regulated exocytosis is highly perturbed in tumor cells, and that the increased number of cells due to the tumor proliferation cannot be responsible alone for the hypersecretion phenotype.

The specific step of the exocytic pathway and which proteins might be involved in this amplified secretory activity remain to be explored in details. However, a significant increase in spike frequency can be consistent with an increase in efficiency of the different steps upstream of the fusion process including recruitment, docking and priming or with a greater calcium sensitivity of the exocytosis machinery. Through the differential mass spectrometry analysis, we have identified several proteins involved in the regulation of these various steps of exocytosis, that are significantly overexpressed in the tumor tissue compared to the non-tumor tissue. Among them, some are known to affect the amperometric spike frequency and/or the kinetics of the spikes when their expression changes in chromaffin cells. This is the case for example of SNARE proteins (SNAP25, Syntaxin1), as well as for

proteins regulating the SNARE complex (Synaptotagmin-1 and -7) or for the actin cytoskeleton organization (Rab27A or Annexin-A2) [45-48].
Fusion pore dynamics is controlled by the competition between fusion pore expansion mechanisms and dynamin-mediated fusion pore closure mechanisms [49] and by specific lipids generated at the exocytotic sites [50]. Faster kinetics of the exocytotic events in tumor cells might be due to a facilitation of the fusion pore expansion which is known to be controlled either by actin-dependent membrane tension [51] and/or by polyunsaturated forms of phosphatidic acid [20]. Whether any of these two pathways is altered in Pheos remains an open question that deserves an in-depth investigation.
Of note, among the core exocytotic machinery, the calcium sensor synaptotagmin-1 was found to be among the most overexpressed in tumor cells (Figure 8), which could lead to an increase in calcium sensitivity and probability of release. Note that we did not find any expression change for membrane calcium channels.

To conclude, we have reported here that calcium-regulated exocytosis is deregulated in human Pheo cells and we have described tumor-associated expression changes of various key players of the exocytic pathway. The next challenge will be to understand how exactly these changes lead to the hypersecretion of catecholamines by the tumors. Moreover, a key unmet need is to find molecules able to prevent the catecholamine hypersecretion directly from the tumor cells. Of note, we have recently identified the somatostatin analog pasireotide (SOM230) as a *bona fide* inhibitor of Pheo hypersecretion [52], but the probable mechanism of action of this drug involves an inhibition of the cholinergic stimulation, which may prove to affect the activity of a large variety of secretory cells possessing nicotinic receptors. There is therefore a need to correct hypersecretion by identifying specific alterations in the secretory machinery whose potential candidates are identified in this study.

Ethics approval and consent to participate

The present study used the data and the human biological material of the biological collection "Approche moléculaire des tumeurs corticosurrénaliennes" which was agreed by the "Comité de Protection des Personnes Est III" ethical advisory committee, and was conducted according to currently accepted ethical guidelines, including informed written consent approval signed by all patients prior to inclusion.

Funding and acknowledgements

This work was financially supported by ITMO Cancer AVIESAN (Alliance Nationale pour les Sciences de la Vie et de la Santé, National Alliance for Life Sciences & Health) within the framework of the Cancer Plan to SG and LB (Single Cell 2018 N° 19CS004-00); by the University of Strasbourg Institute for Advanced Study (USIAS) for a Fellowship, within the French national programme "Investment for the future" (IdEx-Unistra) to SG; by the Conseil Régional de Normandie to CD; by grants from the Agence Nationale pour la Recherche ("SecretoNET", N° ANR-16-CE17-0022-01) and from the Ligue contre le Cancer to SG (CCIR Grand-Est) and to CD (Comité Normand); by a fellowship from la Fondation pour la Recherche Médicale (FRM; FDM201806005916) to SM. INSERM is providing salary to SG and NV.

Conflict of interest

The authors declare that there is no conflict of interest that could be perceived as prejudicing the impartiality of the research reported.

References

[1] W.T. Zandee, K. Kamp, R.C. van Adrichem, R.A. Feelders, W.W. de Herder, Effect of hormone secretory syndromes on neuroendocrine tumor prognosis, Endocr Relat Cancer, 24 (2017) R261-R274.
[2] A. Anantharam, A.J.B. Kreutzberger, Unraveling the mechanisms of calcium-dependent secretion, J Gen Physiol, 151 (2019) 417-434.
[3] R.D. Burgoyne, A. Morgan, Secretory granule exocytosis, Physiol Rev, 83 (2003) 581-632.
[4] T. Lang, R. Jahn, Core proteins of the secretory machinery, Handb Exp Pharmacol, (2008) 107-127.
[5] M.F. Bader, R.W. Holz, K. Kumakura, N. Vitale, Exocytosis: the chromaffin cell as a model system, Ann N Y Acad Sci, 971 (2002) 178-183.
[6] S. Gasman, N. Vitale, Lipid remodelling in neuroendocrine secretion, Biol Cell, 109 (2017) 381-390.
[7] M. Malacombe, M.F. Bader, S. Gasman, Exocytosis in neuroendocrine cells: new tasks for actin, Biochim Biophys Acta, 1763 (2006) 1175-1183.
[8] J.W.M. Lenders, M.N. Kerstens, L. Amar, A. Prejbisz, M. Robledo, D. Taieb, K. Pacak, J. Crona, T. Zelinka, M. Mannelli, T. Deutschbein, H. Timmers, F. Castinetti, H. Dralle, J. Widimsky, A.P. Gimenez-Roqueplo, G. Eisenhofer, Genetics, diagnosis, management and future directions of research of phaeochromocytoma and paraganglioma: a position statement and consensus of the Working Group on Endocrine Hypertension of the European Society of Hypertension, J Hypertens, 38 (2020) 1443-1456.
[9] J.M. Pappachan, N.N. Tun, G. Arunagirinathan, R. Sodi, F.W.F. Hanna, Pheochromocytomas and Hypertension, Curr Hypertens Rep, 20 (2018) 3.
[10] M. Pourian, D.B. Mostafazadeh, A. Soltani, Does this patient have pheochromocytoma? A systematic review of clinical signs and symptoms, J Diabetes Metab Disord, 15 (2015) 11.
[11] R. Zhang, D. Gupta, S.G. Albert, Pheochromocytoma as a reversible cause of cardiomyopathy: Analysis and review of the literature, Int J Cardiol, 249 (2017) 319-323.
[12] H. Fathali, A.S. Cans, Amperometry methods for monitoring vesicular quantal size and regulation of exocytosis release, Pflugers Arch, 470 (2018) 125-134.
[13] E.V. Mosharov, D. Sulzer, Analysis of exocytotic events recorded by amperometry, Nat Methods, 2 (2005) 651-658.
[14] J.W. Lenders, Q.Y. Duh, G. Eisenhofer, A.P. Gimenez-Roqueplo, S.K. Grebe, M.H. Murad, M. Naruse, K. Pacak, W.F. Young, Jr., S. Endocrine, Pheochromocytoma and paraganglioma: an endocrine society clinical practice guideline, J Clin Endocrinol Metab, 99 (2014) 1915-1942.
[15] N.G.S.i.P.S. Group, R.A. Toledo, N. Burnichon, A. Cascon, D.E. Benn, J.P. Bayley, J. Welander, C.M. Tops, H. Firth, T. Dwight, T. Ercolino, M. Mannelli, G. Opocher, R. Clifton-Bligh, O. Gimm, E.R. Maher, M. Robledo, A.P. Gimenez-Roqueplo, P.L. Dahia, Consensus Statement on next-generation-sequencing-based diagnostic testing of hereditary phaeochromocytomas and paragangliomas, Nat Rev Endocrinol, 13 (2017) 233-247.
[16] G. Eisenhofer, J.W. Lenders, D.S. Goldstein, M. Mannelli, G. Csako, M.M. Walther, F.M. Brouwers, K. Pacak, Pheochromocytoma catecholamine phenotypes and prediction of tumor size and location by use of plasma free metanephrines, Clin Chem, 51 (2005) 735-744.
[17] L.D. Thompson, Pheochromocytoma of the Adrenal gland Scaled Score (PASS) to separate benign from malignant neoplasms: a clinicopathologic and immunophenotypic study of 100 cases, Am J Surg Pathol, 26 (2002) 551-566.

[18] S. Moog, S. Houy, E. Chevalier, S. Ory, G. Weryha, M. Rame, M. Klein, L. Brunaud, S. Gasman, T. Cuny, 18F-FDOPA PET/CT Uptake Parameters Correlate with Catecholamine Secretion in Human Pheochromocytomas, Neuroendocrinology, 107 (2018) 228-236.
[19] S. Houy, C. Estay-Ahumada, P. Croise, V. Calco, A.M. Haeberle, Y. Bailly, P. Billuart, N. Vitale, M.F. Bader, S. Ory, S. Gasman, Oligophrenin-1 Connects Exocytotic Fusion to Compensatory Endocytosis in Neuroendocrine Cells, J Neurosci, 35 (2015) 11045-11055.
[20] E. Tanguy, P. Coste de Bagneaux, N. Kassas, M.R. Ammar, Q. Wang, A.M. Haeberle, J. Raherindratsara, L. Fouillen, P.Y. Renard, M. Montero-Hadjadje, S. Chasserot-Golaz, S. Ory, S. Gasman, M.F. Bader, N. Vitale, Mono- and Poly-unsaturated Phosphatidic Acid Regulate Distinct Steps of Regulated Exocytosis in Neuroendocrine Cells, Cell Rep, 32 (2020) 108026.
[21] F. Segura, M.A. Brioso, J.F. Gomez, J.D. Machado, R. Borges, Automatic analysis for amperometrical recordings of exocytosis, J Neurosci Methods, 103 (2000) 151-156.
[22] D.J. Keating, Amperometry in Single Cells and Tissue, Methods Mol Biol, 2233 (2021) 223-231.
[23] E. Lopez-Jimenez, G. Gomez-Lopez, L.J. Leandro-Garcia, I. Munoz, F. Schiavi, C. Montero-Conde, A.A. de Cubas, R. Ramires, I. Landa, S. Leskela, A. Maliszewska, L. Inglada-Perez, L. de la Vega, C. Rodriguez-Antona, R. Leton, C. Bernal, J.M. de Campos, C. Diez-Tascon, M.F. Fraga, C. Boullosa, D.G. Pisano, G. Opocher, M. Robledo, A. Cascon, Research resource: Transcriptional profiling reveals different pseudohypoxic signatures in SDHB and VHL-related pheochromocytomas, Mol Endocrinol, 24 (2010) 2382-2391.
[24] P. Shannon, A. Markiel, O. Ozier, N.S. Baliga, J.T. Wang, D. Ramage, N. Amin, B. Schwikowski, T. Ideker, Cytoscape: a software environment for integrated models of biomolecular interaction networks, Genome Res, 13 (2003) 2498-2504.
[25] D. Szklarczyk, A.L. Gable, K.C. Nastou, D. Lyon, R. Kirsch, S. Pyysalo, N.T. Doncheva, M. Legeay, T. Fang, P. Bork, L.J. Jensen, C. von Mering, The STRING database in 2021: customizable protein-protein networks, and functional characterization of user-uploaded gene/measurement sets, Nucleic Acids Res, 49 (2021) D605-D612.
[26] P. Croise, S. Houy, M. Gand, J. Lanoix, V. Calco, P. Toth, L. Brunaud, S. Lomazzi, E. Paramithiotis, D. Chelsky, S. Ory, S. Gasman, Cdc42 and Rac1 activity is reduced in human pheochromocytoma and correlates with FARP1 and ARHGEF1 expression, Endocr Relat Cancer, 23 (2016) 281-293.
[27] H. Keshishian, T. Addona, M. Burgess, E. Kuhn, S.A. Carr, Quantitative, multiplexed assays for low abundance proteins in plasma by targeted mass spectrometry and stable isotope dilution, Mol Cell Proteomics, 6 (2007) 2212-2229.
[28] M.W. Onaitis, P.M. Kirshbom, T.Z. Hayward, F.J. Quayle, J.M. Feldman, H.F. Seigler, D.S. Tyler, Gastrointestinal carcinoids: characterization by site of origin and hormone production, Ann Surg, 232 (2000) 549-556.
[29] R. Dineen, P.M. Stewart, M. Sherlock, Acromegaly, QJM, 110 (2017) 411-420.
[30] S. Y-Hassan, H. Falhammar, Cardiovascular Manifestations and Complications of Pheochromocytomas and Paragangliomas, J Clin Med, 9 (2020).
[31] R.L. Brown, T. Muzzafar, R. Wollman, R.E. Weiss, A pituitary carcinoma secreting TSH and prolactin: a non-secreting adenoma gone awry, Eur J Endocrinol, 154 (2006) 639-643.
[32] T. Daems, J. Verhelst, A. Michotte, P. Abrams, D. De Ridder, R. Abs, Modification of hormonal secretion in clinically silent pituitary adenomas, Pituitary, 12 (2009) 80-86.
[33] C.C. Juhlin, S. Skoglund, L. Juntti-Berggren, M. Karlberg, J. Calissendorff, Non-functioning neuroendocrine pancreatic tumors transforming to malignant insulinomas - four cases and review of the literature, Neuro Endocrinol Lett, 40 (2019) 175-183.
[34] F. Cuttitta, D.N. Carney, J. Mulshine, T.W. Moody, J. Fedorko, A. Fischler, J.D. Minna, Autocrine growth factors in human small cell lung cancer, Cancer Surv, 4 (1985) 707-727.

[35] P. Song, H.S. Sekhon, Y. Jia, J.A. Keller, J.K. Blusztajn, G.P. Mark, E.R. Spindel, Acetylcholine is synthesized by and acts as an autocrine growth factor for small cell lung carcinoma, Cancer Res, 63 (2003) 214-221.
[36] G. Eisenhofer, T.T. Huynh, A. Elkahloun, J.C. Morris, G. Bratslavsky, W.M. Linehan, Z. Zhuang, B.M. Balgley, C.S. Lee, M. Mannelli, J.W. Lenders, S.R. Bornstein, K. Pacak, Differential expression of the regulated catecholamine secretory pathway in different hereditary forms of pheochromocytoma, Am J Physiol Endocrinol Metab, 295 (2008) E1223-1233.
[37] G. Eisenhofer, T.T. Huynh, M. Hiroi, K. Pacak, Understanding catecholamine metabolism as a guide to the biochemical diagnosis of pheochromocytoma, Rev Endocr Metab Disord, 2 (2001) 297-311.
[38] E. Grouzmann, M. Matter, S. Bilz, A. Herren, F. Triponez, C. Henzen, K.S. Kim, H. Zulewski, T. Buclin, N. Brakch, K. Abid, Monoamine oxidase A down-regulation contributes to high metanephrine concentration in pheochromocytoma, J Clin Endocrinol Metab, 97 (2012) 2773-2781.
[39] K. Isobe, T. Nakai, N. Yukimasa, T. Nanmoku, K. Takekoshi, F. Nomura, Expression of mRNA coding for four catecholamine-synthesizing enzymes in human adrenal pheochromocytomas, Eur J Endocrinol, 138 (1998) 383-387.
[40] B. Jarrott, W.J. Louis, Abnormalities in enzymes involved in catecholamine synthesis and catabolism in phaeochromocytoma, Clin Sci Mol Med, 53 (1977) 529-535.
[41] G. Eisenhofer, I.J. Kopin, D.S. Goldstein, Catecholamine metabolism: a contemporary view with implications for physiology and medicine, Pharmacol Rev, 56 (2004) 331-349.
[42] J.W. Lenders, G. Eisenhofer, N.G. Abeling, W. Berger, D.L. Murphy, C.H. Konings, L.M. Wagemakers, I.J. Kopin, F. Karoum, A.H. van Gennip, H.G. Brunner, Specific genetic deficiencies of the A and B isoenzymes of monoamine oxidase are characterized by distinct neurochemical and clinical phenotypes, J Clin Invest, 97 (1996) 1010-1019.
[43] A. Saveanu, M. Muresan, C. De Micco, D. Taieb, A.L. Germanetti, F. Sebag, J.F. Henry, L. Brunaud, A. Enjalbert, G. Weryha, A. Barlier, Expression of somatostatin receptors, dopamine D(2) receptors, noradrenaline transporters, and vesicular monoamine transporters in 52 pheochromocytomas and paragangliomas, Endocr Relat Cancer, 18 (2011) 287-300.
[44] M. Guerin, J. Guillemot, E. Thouennon, A. Pierre, F.Z. El-Yamani, M. Montero-Hadjadje, C. Dubessy, R. Magoul, I. Lihrmann, Y. Anouar, L. Yon, Granins and their derived peptides in normal and tumoral chromaffin tissue: Implications for the diagnosis and prognosis of pheochromocytoma, Regul Pept, 165 (2010) 21-29.
[45] C. Desnos, J.S. Schonn, S. Huet, V.S. Tran, A. El-Amraoui, G. Raposo, I. Fanget, C. Chapuis, G. Menasche, G. de Saint Basile, C. Petit, S. Cribier, J.P. Henry, F. Darchen, Rab27A and its effector MyRIP link secretory granules to F-actin and control their motion towards release sites, J Cell Biol, 163 (2003) 559-570.
[46] Q. Fang, K. Berberian, L.W. Gong, I. Hafez, J.B. Sorensen, M. Lindau, The role of the C terminus of the SNARE protein SNAP-25 in fusion pore opening and a model for fusion pore mechanics, Proc Natl Acad Sci U S A, 105 (2008) 15388-15392.
[47] M. Gabel, F. Delavoie, V. Demais, C. Royer, Y. Bailly, N. Vitale, M.F. Bader, S. Chasserot-Golaz, Annexin A2-dependent actin bundling promotes secretory granule docking to the plasma membrane and exocytosis, J Cell Biol, 210 (2015) 785-800.
[48] B. Tawfik, J.S. Martins, S. Houy, C. Imig, P.S. Pinheiro, S.M. Wojcik, N. Brose, B.H. Cooper, J.B. Sorensen, Synaptotagmin-7 places dense-core vesicles at the cell membrane to promote Munc13-2- and Ca(2+)-dependent priming, Elife, 10 (2021).
[49] W.D. Zhao, E. Hamid, W. Shin, P.J. Wen, E.S. Krystofiak, S.A. Villarreal, H.C. Chiang, B. Kachar, L.G. Wu, Hemi-fused structure mediates and controls fusion and fission in live cells, Nature, 534 (2016) 548-552.

[50] E. Tanguy, O. Carmon, Q. Wang, L. Jeandel, S. Chasserot-Golaz, M. Montero-Hadjadje, N. Vitale, Lipids implicated in the journey of a secretory granule: from biogenesis to fusion, J Neurochem, 137 (2016) 904-912.
[51] W. Shin, L. Ge, G. Arpino, S.A. Villarreal, E. Hamid, H. Liu, W.D. Zhao, P.J. Wen, H.C. Chiang, L.G. Wu, Visualization of Membrane Pore in Live Cells Reveals a Dynamic-Pore Theory Governing Fusion and Endocytosis, Cell, 173 (2018) 934-945 e912.
[52] L. Streit, S. Moog, S. Hugel, M. Rame, E. Tanguy, V. Andry, H.A. Schmid, L. Brunaud, F. Bihain, C. Nomine-Criqui, Y. Goumon, S. Lacomme, S. Lomazzi, M. Vix, D. Mutter, N. Vitale, S. Ory, S. Gasman, Somatostatin analogue pasireotide (SOM230) inhibits catecholamine secretion in human pheochromocytoma cells, Cancer Lett, (2021).